Journal of Power Sources 234 (2013) 91–99

Contents lists available at SciVerse ScienceDirect

Journal of Power Sources

journal homepage: www.elsevier.com/locate/jpowsour

Integration of solid-state dye-sensitized solar cell with metal oxide charge storage material into photoelectrochemical capacitor

Magdalena Skunik-Nuckowska [a], Katarzyna Grzejszczyk [a], Pawel J. Kulesza [a,*], Lei Yang [b], Nick Vlachopoulos [b], Leif Häggman [b], Erik Johansson [b], Anders Hagfeldt [b]

[a] University of Warsaw, Department of Chemistry, Pasteura 1, PL-02-093 Warsaw, Poland
[b] Department of Physical and Analytical Chemistry, Uppsala University, Box 259, SE-751 05 Uppsala, Sweden

HIGHLIGHTS

- An integrated microelectrochemical device for solar energy storage is reported here.
- The system defined as *photocapacitor* consists of dye solar cell and supercapacitor.
- The device operates under various light conditions including low light intensity.
- Energy conversion efficiency (including storage) of 0.8% has been obtained.

ARTICLE INFO

Article history:
Received 16 October 2012
Received in revised form
29 December 2012
Accepted 16 January 2013
Available online 26 January 2013

Keywords:
Photocapacitor
Dye-sensitized solar cell
Poly-(3-hexylthiophene-2,5-diyl)
Supercapacitor
Ruthenium oxide
Optoelectronics

ABSTRACT

A solid-state photo-rechargeable capacitor (photocapacitor) is obtained here by coupling a dye-sensitized solar cell and a ruthenium oxide based electrochemical capacitor. This integrated system permits direct storage of energy generated by sunlight within a single optoelectronic micro-electrochemical device. It utilizes three planar electrodes arranged sequentially to include a polymer hole conductor (poly-(3-hexylthiophene-2,5-diyl)), between the titanium oxide photoanode modified with dye (*E*)-3-(5-(4-(Bis(20,40-dibutoxybiphenyl-4-yl)amino)phenyl)thiophen-2-yl)-2-cyanoacrylic acid (D35) and the intermediate silver electrode as well as two hydrous ruthenium oxide layers (separated by protonically conducting Nafion™ membrane) between the intermediate (silver) and the external (counter) electrode. Upon integration of the capacitor and dye-sensitized solar cell into a single photocapacitor hybrid device, the following parameters were obtained under simulated 100 mW cm^{-2} solar illumination: specific capacitance, 407 F g^{-1} (3.26 F cm^{-2}); energy and power densities, 0.17 mWh cm^{-2} and 0.34 mW cm^{-2} and coulombic efficiency, 88%. These data together with results of experiments performed at different light intensities (10–100 mW cm^{-2}) are consistent with very good performance of the optoelectronic device under various light conditions.

1. Introduction

There has been a growing recent interest in the development of photovoltaic cells utilizing dyes adsorbed on the nanostructured semiconductor metal oxide, mostly titanium dioxide electrodes as low-cost alternatives to traditional silicon based solar cells. Since the invention of dye-sensitized solar cells (DSSC) in early 1990s [1], their efficiency has been significantly improved up to 11% [2] or even to 12.3% for certain prototypes [3]. Most of practical designs feature ruthenium based dyes over-coating high surface area anatase (TiO_2) films existing in combination with liquid, or semi-liquid, redox-conducting electrolytes composed of the iodide/triiodide couple dissolved in various organic media. Such DSSC designs suffer from numerous disadvantages that include strong temperature effects and related problems with electrolyte freezing or crystallization and leaking or evaporation at low and high temperatures, respectively. The corrosive (oxidative) properties of iodine (especially in the presence of water and oxygen), as well as the utilization of toxic and volatile solvents (e.g. acetonitrile) should also be mentioned here. Therefore, a great effort has been made to replace liquids by solid state materials such as polymeric electrolytes [4], electronically conducting polymers [5–12], p-type inorganic semiconductors like copper thiocyanates or iodides [13–17], (2,20,7,70-tetrakis (*N*,*N*-dimethoxyphenylamine)-9,90-spirobifluorene) (spiro-OMe-TAD) [18–24] or mixed-valent redox-conducting Prussian blue type

* Corresponding author. Tel.: +48 8220211x289; fax: +48 228225996.
E-mail address: pkulesza@chem.uw.edu.pl (P.J. Kulesza).

0378-7753/$ – see front matter © 2013 Elsevier B.V. All rights reserved.
http://dx.doi.org/10.1016/j.jpowsour.2013.01.101

nickel hexacyanoferrates [25,26]. In principle, solid-state DSSCs are easier to assemble and their long-term stabilities are higher due to lower chances for the unexpected electrolyte leakages or the dye desorption and degradation phenomena. Solid-state systems would obviously be preferred when it comes to possible applications of DSSCs, e.g. to the development of optoelectronic devices. Until now, the energy conversion efficiency of solid state DSSCs is still lower in comparison to the liquid iodide/triiodide based cells, but recent attempts resulting in the efficiency exceeding 7% [21,27] should be noted here.

Storage and effective utilization of generated energy is also an important issue for solar cell technology. A possibility of charge storage within an electrochemical secondary battery introduced as a part of DSSC has been reported [28–31]. An electrochemical capacitor, or supercapacitor, offers advantage of the high power density together with long-term stability during repetitive charging/discharging cycles [32–34]. Moreover, high energy densities can be achieved by deliberate combination of the electric double layer charging/discharging (e.g. with use of high surface area nanostructured carbons) with the so called pseudo-capacitance effects originating from fast redox (Faradic) reactions appearing at the electrochemical interfaces [33].

Here we report on fabrication and characterization of the photoelectrochemical capacitor (photocapacitor) obtained by coupling the solid state dye-sensitized solar cell with the semi-solid symmetrical redox supercapacitor. We refer here to the recent concepts of preparation of the photo-charging type capacitor as a single system rather than parallel combination of two separate devices, a photocell and a capacitor. This interesting and fairly new concept was for the first time proposed by Miyasaka et al. [35]. The simple two-electrode photocapacitor cell based on activated carbon as charge storage material was characterized by capacitance of 0.69 F cm^{-2}, coulombic efficiency of 59% and capacitor potential window of 0.4 V. The device was composed of TiO_2/dye photoelectrode coated with solid hole conductor (LiI), platinum-covered counter electrode and two activated carbon based layers inserted between and separated by liquid ionic electrolyte. Our initial work with the similar type two-electrode system [36] showed two main drawbacks: (i) high internal resistance of semiconductor photoelectrode intervening with the discharging step, and (ii) cross-over of iodide or iodine into inert electrolyte in the charge storage compartment leading to short-circuiting and self-discharging problems.

More advanced designs based on three-electrode configurations [37–39], in which an intermediate bipolar electrode was in contact with the charge-transport medium of DSSC on one side and the charge-storage supercapacitor material on the other one, were also proposed. These systems utilized liquid-type DSSC cells with I^-/I_3^- redox couples as charge relays.

In the present work, we report on preparation of the solid-state type microelectrochemical system in which photoelectrochemical energy conversion and charge storage functions are integrated within a single planar optoelectronic device. While the light harvesting part is based on D35 dye [40] as a sensitizer over-coating TiO_2, the charge relay is used in a form of hole-conducting conjugated polymer, namely poly-(3-hexylthiophene-2,5-diyl), P3HT [19]. The polymer film has an evaporated silver layer which adheres well under high vacuum, and serves both as the counter electrode and the bipolar layer contacting and supporting the capacitor part.

Ruthenium oxide, $RuO_x(OH)_y$ widely known as the mixed-valence redox conducting material capable of fast charge (electron, proton) propagation in the solid (or semi-solid, i.e. hydrated state), has been selected as an effective charge-storage material [41,42]. The sol–gel processed ruthenium oxide in its hydrous and amorphous forms has been carefully dispersed together with carbon black and Nafion™ binding solution to achieve maximum storage abilities as well as high electrical/ionic conductivity. A proton-conducting polymer membrane has been used as a semi-solid electrolyte (separator).

The resulting photocapacitor has been illuminated under different light intensities (10–100 mW cm^{-2}) and, subsequently, discharged in a galvanostatic mode at different current densities. The system parameters, such as voltage, specific capacitance, energy and power densities, as well as energy conversion and coulombic efficiencies are reported here and found attractive in comparison to literature data [35,37–39].

2. Experimental

2.1. Fabrication and characterization of solid-state DSSC

A compact TiO_2 blocking layer was deposited onto the surface of a pre-cleaned fluorine-doped tin oxide glass, FTO (2.2 mm thick, resistance of 15 Ω/square, Solaronix, Switzerland) substrate by spray pyrolysis on a hotplate at 450 °C using an airbrush at a distance of 5 cm. The thickness was controlled by the number of spray cycles. The solution used in the spray pyrolysis was 0.2 mol dm^{-3} titanium isopropoxide (Sigma–Aldrich, USA) and 2 mol dm^{-3} acetylacetone in isopropanol. 10 spray cycles were used in standard procedure. Nanoporous TiO_2 films were prepared on the compact TiO_2 layer by spin-coating a colloidal TiO_2 paste (DSL 18NR-T, Dyesol, Australia) containing nanoparticles in the order of 20 nm in diameter diluted in terpineol (41.7% weight ratio). A spin-coating rate of 2500 rpm for 30 s was adopted to obtain about 2 mm thick nanoporous film, as measured with a DekTak profilometer and SEM. After sintering the TO_2 film on a hotplate at 450 °C for 30 min, the film was cooled to room temperature and immersed in 0.02 mol dm^{-3} aqueous $TiCl_4$ (Sigma–Aldrich) at 70 °C for 30 min. The film was then rinsed with deionized water and annealed on a hotplate at 450 °C for 30 min. After cooling to 90 °C, it was immersed for 18 h in 0.2 mmol dm^{-3} solution of D35 dye ((*E*)-3-(5-(4-(bis(20,40-dibutoxybiphenyl-4-yl) amino)phenyl)thiophen-2-yl)-2-cyanoacrylic acid, synthesized as described elsewhere [52]) in ethanol. In the next step a solution of P3HT (MW 15 000–45 000, Sigma–Aldrich, USA), 20 mg cm^{-3} in chlorobenzene was prepared in an Argon glovebox. The solution was prepared with the additives of 60 mmol dm^{-3} 4-tert-butylpyridine (Sigma–Aldrich, USA) and 15 mmol dm^{-3} lithium trifluoromethanesulfonate (Sigma–Aldrich, USA) and was applied on TiO_2 films. After waiting for 1 min a spin-coating for 30 s with 2000 rpm was adopted. Finally, a silver contact was deposited onto the organic semiconductor by thermal evaporation in a vacuum chamber (Leica EM MED020) with a base pressure of about 10^{-5} mbar, to complete the cell. The active area was 0.2 cm^{-2}.

IPCE spectra were recorded on a computer-controlled setup comprised of a xenon lamp (Spectral Products ASB-XE-175), a monochromator (Spectral Products CM110) and a potentiostat (EG&G PAR 273). The setup was calibrated with a certified silicon solar cell (Fraunhofer ISE) prior to measurements. The sample was illuminated from the glass side with an aperture area of 0.16 cm^2 (0.4 × 0.4 cm^2).

A sample of DSSC was imaged by scanning electron microscopy (SEM). It was scribed on the substrate (glass) side and cracked prior to acquisition of the SEM images (Zeiss LEO1550 high resolution SEM). The acceleration voltage (EHT) was 10 kV and the working distance (WD) ranged from 12 to 13.5 mm. Entire cross sections were imaged at a magnification of 50,000×.

2.2. Preparation of $RuO_x(OH)_y$ based materials for capacitor electrodes

Ruthenium oxide was prepared by a sol–gel method using a procedure described elsewhere [41]. In the first step, 0.1 mol dm^{-3}

aqueous solution of $RuCl_3$ (Ru, 38% min.; Alfa Aesar, USA) was carefully mixed with 0.3 mol dm^{-3} solution of NaOH (Polish Chemicals Reagents, POCH, Poland) until pH = 7. As a result, a deep brown precipitate of ruthenium hydroxide appeared readily. A solid product was filtered, washed thoroughly with distilled water and ethanol and, finally, annealed for 17 h at 150 °C in air to convert the hydroxide into amorphous and hydrated form of oxide, $RuO_x(OH)_y$.

To fabricate composite materials for capacitor electrodes, a suspension containing 60 mg of $RuO_x(OH)_y$, 30 mg of Nafion™ solution (5% in lower aliphatic alcohols and water, Sigma–Aldrich, USA) and 10 mg of acetylene black (Alfa Aesar, USA) was prepared in ethanol. To make the suspension homogeneous, it was first placed in the ultrasound bath for 30 min and, then, exposed to magnetic stirring for 12 h. The fairly dense ink-type suspension thus prepared was spread uniformly using micropipette onto carbon paper substrate (Toray; thickness, 190 μm, Electrochem. Inc., USA) cut into circles of 5.7 cm^2 area and placed in a Büchner funnel under vacuum pump conditions. The immobilized material was rinsed several times with water and ethanol, dried at 60 °C and cut into rectangular pieces (active area of the cell was 0.2 cm^2). The mass of the composite material deposited on each carbon paper electrode was estimated from the mass differences of bare and covered carbon substrates. Carbon paper served here as both support for the electroactive material and current collector.

Two electrodes of similar weight were subsequently assembled face-to-face and separated by Nafion™ 117 membrane (thickness, 180 μm; from Alfa Aesar, USA) which served as proton-conductive solid electrolyte. The membrane was first pretreated by gentle boiling at 80 °C in 0.5 mol dm^{-3} H_2SO_4 and de-ionized water each time for 1 h. Thus prepared membrane was stored in water for further use. To assemble a cell and achieve a good electrical contact between carbon paper electrodes modified with ruthenium oxide and polymer electrolyte, all the parts of the cell were hot-pressed for 5 min at 125 °C under 12 kg cm^{-2} pressure. To convert the membrane into fully protonated form before use, the cell was immersed in hot 0.5 mol dm^{-3} H_2SO_4 for at least 1 h and, then, rinsed carefully with distilled water.

All electrochemical measurements involving capacitors were performed by immobilizing the cell between two glass plates covered FTO. A self-adhesive Scotch® gasket was inserted between the plates to prevent short-circuiting. Electrochemical characterization was carried out using CH 660C Workstation (Austin/Texas, USA). The capacitor's performance was examined using cyclic voltammetry (at scan rates ranging from 2 to 100 mV s^{-1}), and the galvanostatic charging-discharging technique (current densities ranging from 0.8 to 12.8 mA cm^{-2} which corresponded to 100–1600 mA g^{-1}). In calculations, geometric area of capacitor (0.2 cm^2) and total mass of active electrode material at one electrode (1.6 mg) excluding the carbon paper support were taken into account.

2.3. Fabrication and testing of integrated photocapacitor

A design of three-electrode photocapacitor cell is shown in Fig. 1. The device consists of two external FTO electrodes. One of them, photoanode (on left side in Fig. 1) is in contact with the light-harvesting system of porous TiO_2 modified with D35 dye and coated with P3HT hole conducting polymer (charge relay). As a rule, the photoanode is over-coated with thin layer of silver by vacuum evaporation. This intermediate bipolar silver electrode is also in contact with the charge-storage capacitor material, $RuO_x(OH)_y$ on the other (right in Fig. 1) side (while being in contact with solid hole conductor (P3HT) on the left side). The external FTO plates (electrodes) are separated by self-adhesive tape gaskets to avoid short circuiting from direct contact with conducting glass plates.

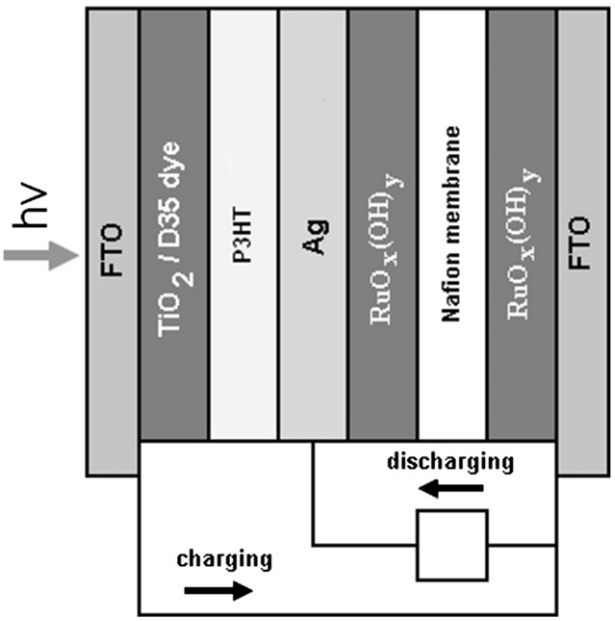

Fig. 1. Schematic presentation of three-electrode solid-state integrated photocapacitor consisting of two (DSSC and electrochemical capacitor) parts. A vacuum-evaporated Ag layer serves as the intermediate bipolar electrode. The external photoanode (on the left) is from TiO_2-covered FTO glass subsequently modified with D35 dye. The external counter electrode (on the right) consists of FTO glass. The P3HT conducting polymer acts as a charge relay. Two ruthenium oxide layers are separated by a Nafion™ proton-conducting membrane. Charging and discharging steps as well as electron flow direction are marked with arrows.

It is apparent from the scheme (Fig. 1) that the photocharging step utilized two external FTO electrodes which were connected to the potentiostat operating in two-electrode mode. To execute charging, the device was subjected to short-circuit amperometric experiment at 0 V under different light intensity values in the range 10–100 mW cm^{-2}. During the charging process, the voltage across the capacitor part (between intermediate silver and external FTO electrodes) was monitored using an electrometer. The charged photocapacitor was left each time for 60 s under open circuit conditions and, subsequently, discharged in the galvanostatic mode by applying the series of increasing current densities from 0.8 to 12.8 mA cm^{-2}. To perform photocapacitor tests, a white diode spotlamp (parameters: 700 mA, 4.47 V; VLM, Italy) equipped with cut-off filters capable of removing infrared and ultraviolet radiation was used as a source of light. The lamp was calibrated to the desired light intensity with use of a visible-light-sensitive silicon-photocell (Vishay Intertechnology, USA). The same light source was used for DSSC operating independently without capacitor part (Fig. 2).

3. Results and discussion

3.1. Operation and characterization of solid-state dye-sensitized solar cell

Fig. 2A (solid line) illustrates a typical current-potential response of the TiO_2/D35/P3HT/Ag photocell (in which TiO_2 photoanode is modified with D35 dye, P3HT serves as the charge relay, and the Ag over-layer acts as the counter electrode) following illumination with the simulated sunlight of 100 mW cm^{-2}. For a series of samples, we have obtained short circuit photocurrent densities between 5 and 7 mA cm^{-2} which corresponds to energy conversion efficiency (η) between 2 and 3% depending on the individual sample preparation and storage. It is important to note

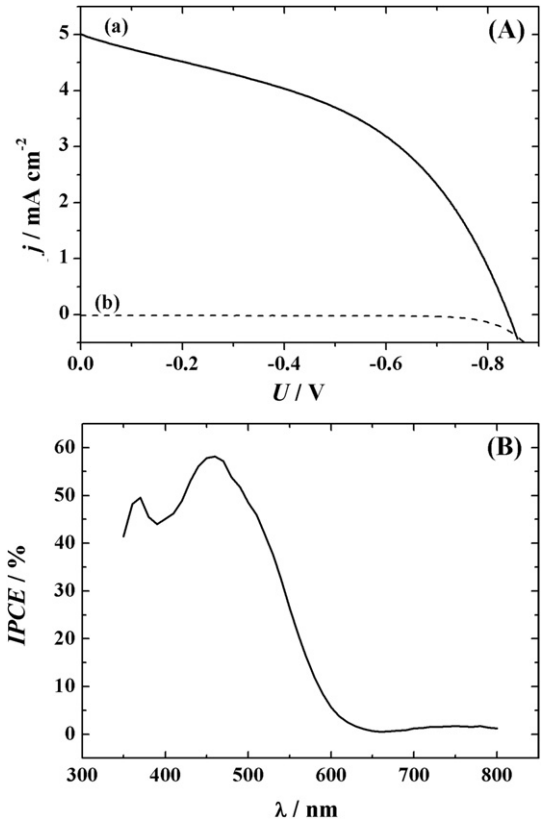

Fig. 2. Diagnosis of solid-state DSSC utilizing a D35 dye modified TiO_2 based photoanode, a P3HT conducting polymer as charge-transport layer and a silver layer cathode. (A) Monitoring of current density (j) *vs.* applied potential difference (ΔV) under illumination with 100 mW cm^{-2} simulated AM 1.5 sunlight (a) and in the dark (b). (B) Spectrum of Incident Photon to Current Efficiency (IPCE) *vs.* wavelength (λ) recorded for the above cell.

that all the samples display high open circuit voltages exceeding 0.8 V. This parameter is certainly not lower but, on average, ca. 0.1 V higher in comparison to the performance of the liquid-type DSSC utilizing D35 dye as reported elsewhere [42]. Further, despite the fact that the cell has operated under truly dry (solid-state) conditions, the shape of the current–potential curve (Fig. 2A) does not imply ohmic limitations.

Spectroscopic characteristics, namely the incident photon-to-current conversion efficiency (IPCE) spectrum of the TiO_2/D35/P3HT/Ag photocell, are presented in Fig. 2B. The result is consistent with a moderately high conversion efficiency while the action spectrum is characterized by a peak reaching the maximum IPCE value of 58% at 460 nm. Knowing that the FTO electrode transmits about 90% of sunlight in the investigated spectral region, the absorbed photon-to-current conversion efficiency (APCE) is estimated to be close to 70%. To our best knowledge, this result is one of the highest reported so far for a solid-state-type DSSC utilizing conducting polymers as a hole conductor.

To examine morphology of the photocapacitor cell, cross-sectional measurements have been performed using scanning electron microscopy (Fig. 3). Here the presence of a mesoporous TiO_2 layer of approximately 1 μm thickness is clearly visible. Between the semiconducting TiO_2 layer and the intermediate silver electrode, a thin (ca. 200 nm) layer of hole conductor, namely the P3HT conducting polymer, can be seen. Obviously, the porous TiO_2 structure is probably not completely filled with the polymeric material. Thus, as recently postulated [19], only a certain portion of dye molecules is likely to be in direct contact of with the polymer

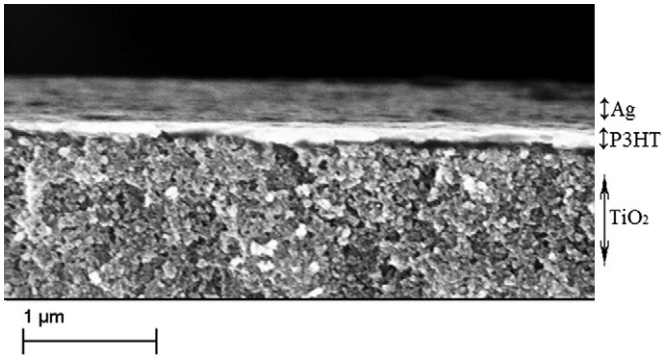

Fig. 3. Cross sectional view of DSSC cell (as for Fig. 2) obtained by scanning electron microscopy.

charge relay. This situation may translate to incomplete dye reduction during the regeneration process within the DSSC. This phenomenon obviously limits the overall performance of the polymer based solid-state DSSC which was discussed in details previously [19].

3.2. Performance of solid-state photoelectrochemical capacitor

To comment on the usefulness of hydrous ruthenium oxide as a redox-conducting pseudocapacitive material for applications under solid-state electrochemical conditions in the absence of contact with liquid supporting electrolyte, a series of voltammetric and galvanostatic experiments were conducted in the two-electrode configuration. Fig. 4A shows a typical dependence of specific capacitance (C) on applied potential that has been recorded for a symmetrical-type capacitor in which two ruthenium oxide layers are separated by a Nafion™ proton-conducting membrane (semi-solid electrolyte). In this respect the C value is expressed per mass of a single composite electrode, and it has been calculated according to the formula:

$$C = 2\frac{i}{v \cdot m} \quad (1)$$

where C is in F g^{-1}, i stands for voltammetric current (A), v is a scan rate (V s^{-1}), m is equivalent to mass of the active material of one electrode (g).

It is noteworthy that, during both oxidation and reduction scans, specific capacitances reach very high values exceeding 400 F g^{-1} with respect to the whole mass of composite electrode (Fig. 4A); the result translates into 665 F g^{-1} of $RuO_x(OH)_y$ present on a single electrode. This value is close to that previously reported (768 F g^{-1}) for similar systems but operating in liquid electrolyte (H_2SO_4) [43]. In addition, the rectangular shape of the response in Fig. 4A is consistent with good capacitive behavior and fairly fast dynamics of charging/discharging processes characterized by rather low ohmic limitations. For the cells utilizing Nafion™ membranes, the box-like shaped voltammetric curves of Fig. 4A can only be recorded upon application of scan rates not exceeding 20 mV s^{-1} (contrary to the systems with sulfuric acid where the scan rate limit is up to at least up to 50 mV s^{-1} [43]). Indeed, aqueous inorganic electrolytes are known to provide low internal resistance attributed to their high ionic conductivity. Although the Nafion™ membrane is characterized by fairly high proton conductivity (ca. 0.1 S cm^{-2} at ambient temperature [47–50]), the mobility of protons within Nafion™ membrane is obviously lower than in aqueous H_2SO_4. The capacitive properties of ruthenium oxide are strongly influenced by proton mobility because charging of oxide is strictly dependent on

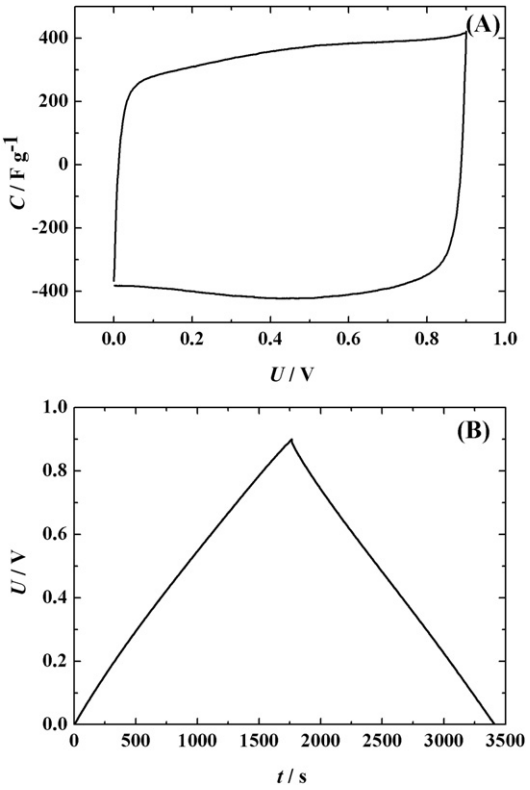

Fig. 4. Diagnosis of solid-state photoelectrochemical capacitor part. (A) Dependence of specific capacitance (C) as a function of applied potential (E) for $RuO_x(OH)_y$ based supercapacitor utilizing Nafion™ membrane obtained from cyclic voltammetric (scan rate 2 mV s^{-1}) data. (B) Galvanostatic charging/discharging, i.e. monitoring of capacitor's voltage *vs.* time (t) upon application of 0.8 mA cm^{-2} (100 mA g^{-1}). Mass and area of each electrode were 1.6 mg and 0.2 cm^{-2}, respectively.

the reversible protonation/deprotonation process [44,45]. Thus oxidation states of ruthenium can change from II to IV; in this respect it should be recalled that the $Ru^{II}(OH)_2$ form exists at 0 V and $Ru^{IV}O_2$ exists at 1.4 V versus standard hydrogen electrode (SHE) [46]. Because the maximum charging voltage of our two-electrode symmetric capacitor does not exceed 0.9 V, it is reasonable to expect that when the mixed-valent $Ru^{IV,\,III}O_x$, rather than $Ru^{IV}O_2$, is formed. Thus it can be concluded that, although the performance of ruthenium oxide is not fully optimized under solid-state conditions, the system's charging/discharging processes are quite fast and lead to high specific capacitances with use of Nafion™ membrane.

More information about the capacitor performance was obtained from galvanostatic charging/discharging experiments. A typical galvanostatic charging/discharging profile for ruthenium oxide based solid-state capacitor is shown in Fig. 4B. The experiment was performed at a low current density of 0.8 mA cm^{-2} which corresponds to 100 mA g^{-1} (with respect to the total mass of a single electrode material).

The specific capacitance was determined using the typical equation:

$$C = 2 \cdot \frac{i_{dch} \cdot t_{dch}}{U_{dch} \cdot m} \quad (2)$$

where meaning of parameters is as follows: C – specific capacitance (F g^{-1}), i_{dch} – discharge current (A), t_{dch} – discharge time (s), U_{dch} – discharge voltage decreased by the ohmic drop (V), and m – total mass of one electrode (g).

The specific capacitance calculated on the basis of above equation was 370 F g^{-1} (2.96 F cm^{-2}) that corresponds to energy density of 10.4 Wh kg^{-1} (0.166 mWh cm^{-2}) and power density of 22.7 W kg^{-1} (0.36 mW cm^{-2}). All parameters were determined by the usual means [51]. In the calculations, the total mass (3.2 mg) and the experimentally determined capacitance of each composite electrode was taken into account. Finally, upon increasing of the charging/discharging current density up to 12.8 mA cm^{-2} (1600 mA g^{-1}), only a ca. 20% drop in capacitance has been observed. The result implies that the system is well-behaved, and it is characterized by fairly fast dynamics of charge propagation as well as reversibility of charging and discharging steps.

3.3. Operation of integrated solid-state photocapacitor device

In order to investigate on photocharging capabilities of the integrated microelectrochemical photocapacitor, the device was irradiated under visible light of varying intensity, ranging from 10 to 100 mW cm^{-2} (equivalent to 10–100% sunlight) while short-circuited, by connecting two outer FTO plates (Fig. 1), to the potentiostat operating in two-electrode mode. The results are summarized in Fig. 5. Simultaneous changes in current densities between the external FTO electrodes (Fig. 5A and B) as well as the generated voltage changes across capacitor, i.e. between the intermediate silver electrode and the external FTO electrode being in contact with $RuO_x(OH)_y$ layer (Fig. 5C), were monitored. In this respect the charging voltage was measured point by point using an electrometer. Typical photocharging curves are shown in Fig. 5A. When the light was switched on, the photocurrent was generated rapidly to reach values of 3.9, 1.8 and 0.38 mA cm^{-2} depending on the light intensity (100, 50 and 10% of full sunlight, respectively). The results are close to what one would expect from the performance of the same DSSC operating independently (Fig. 2). Obviously, current generated in a photocapacitor does not remain stable as in a typical DSSC, but decays exponentially with time. The same phenomenon can be observed during charging of the electrochemical capacitor at constant voltage. When current starts to decrease, the voltage (U) across the capacitor begins to increases immediately (Fig. 5C) and reaches the following values: 898, 829 and 762 mV (for light intensities, 100, 50 and 10% of full sunlight, respectively, as summarized in Table 1). As a rule, photocharging was stopped when the voltage on electrometer reached the maximum value. The observation indicated that maximum possible amount of charge was accumulated inside the capacitor part. In general, when the higher light intensity was applied (higher charging photocurrent generated), faster charging was observed. Indeed, the photocharging times (t_{ch}) were equal to 800, 1860 and 5850 s for light intensities of 100, 50 and 10% of full sunlight (Table 1). Although the charging step was rather prolonged at the lowest light intensity, it still yielded a reasonable voltage across the capacitor. That observation implies that our integrated capacitor can be potentially used under the indoor, cloudy or limited sunlight conditions.

The anodic-type character of photocurrent responses suggests that the generated electrons flow directly from the photoelectrode to the positively charged counter electrode where they are stored and responsible for electrochemical charging of the neighboring $RuO_x(OH)_y$ layer. Having in mind concepts of operation of typical DSSC's, the charging mechanism can be proposed as follows. The first step involves photoexcitation of the dye (D35) molecules followed by generation of electrons (Equation (3)) that are subsequently injected to the TiO_2 conduction band.

$$D35 \xrightarrow{h\nu} D35^* \rightarrow D35_{ox} + e^- \quad (3)$$

Later, electrons flowing through the external circuit to the surface of the FTO counter electrode and holes generated within the

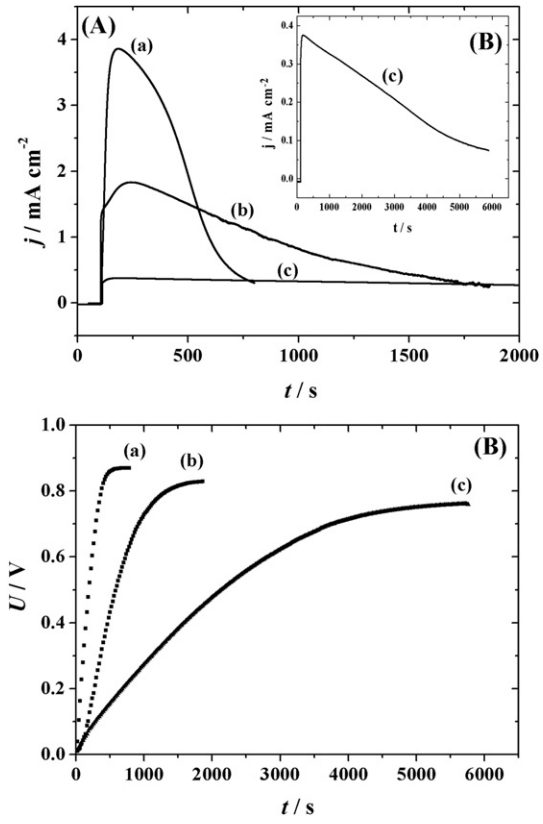

Fig. 5. Photocharging of integrated photocapacitor. (A) Monitoring (at 0 V) of current density (j) *vs.* time during photocharging during amperometric experiment utilizing two external electrodes under different light intensity values: (a) 100, (b) 50, and (c) 10 mW cm^{-2} (equivalent to 100, 50 and 10% of full sun, respectively). Inset (B) illustrates curve c upon expanding the time scale to 6000 s. (C) Monitoring of the capacitor's voltage (U) between the silver electrode and the external counter electrode (Fig. 1) *vs.* time of photocharging (recorded with experimental conditions as for Fig. 5A). Illumination parameters for curves a, b and c are as above.

dye are replaced by the electrons originating from the appropriate charge relay. Consequently, the solid polymer hole conductor, P3HT, that is utilized here, becomes positively charged (Equation (4)):

$$D35_{ox} + P3HT \rightarrow D35_{red} + P3HT_{ox} \quad (4)$$

Thus oxidized hole conductor is subsequently reduced (regenerated) to its initial form at the surface of the intermediate (Ag) electrode thus resulting in the simultaneous oxidation of ruthenium oxide material (Equation (5)) and storage of positive charge in the neighboring capacitor layer being in contact with the silver electrode:

$$P3HT_{ox} + RuO_x(OH)_y \rightarrow P3HT + RuO_{x+\delta}(OH)_{y-\delta} \quad (5)$$

Simultaneously electrons flowing through the external circuit to the surface of the FTO external counter electrode are accumulated there as negative charges which results in the reduction of the $RuO_x(OH)_y$ layer being in contact with the conductive glass (Equation (6)):

$$RuO_x(OH)_y + \delta H^+ + \delta e^- \rightarrow RuO_{x-\delta}(OH)_{y+\delta} \quad (6)$$

When the supercapacitor is fully charged, two different ruthenium oxide forms (separated by the Nafion™ membrane) co-exist: oxidized at the silver electrode, and reduced at the counter electrode. The total amounts of charge accumulated in the integrated photocapacitor following photocharging (Q_{ch}) are given in Table 1. The values varied from 1.22 to 1.64 C cm^{-2} depending on the light intensity. When compared to other photocapacitor-type systems, the present value obtained under the 100% sunlight is 32% higher than that reported earlier [37] and only 25% lower than that reported more recently [38] (Table 3).

When the voltage across the capacitor reached its maximum value, the photocharging was stopped and the photoelectrode was disconnected. After 60 s of rest time, the capacitor part was subjected to galvanostatic discharging at 0.8 mA cm^{-2} (Fig. 6A). The rest time always caused some voltage drop (Table 1) due to internal resistance (ohmic drop) as well as to self-discharge processes. The differences between the voltage at the end of the charging process and after a rest time are marked in Table 1 as U and U_{dch}.

The reactions occurring at the capacitor electrodes during discharging can be described in terms of the following reactions:

$$RuO_{x+\delta}(OH)_{y-\delta} + \delta H^+ + \delta e^- \rightarrow RuO_x(OH)_y \quad \text{at the silver (positive) electrode} \quad (7)$$

$$RuO_{x-\delta}(OH)_{y+\delta} \rightarrow RuO_x(OH)_y + \delta H^+ + \delta e^- \quad \text{at the external (negative) electrode} \quad (8)$$

From the galvanostatic curve obtained at 0.8 mA cm^{-2} (Fig. 6A), the values of capacitance per geometric area of the capacitor electrode as well as per total mass of one electrode were estimated from the galvanostatic curves recorded at 0.8 mA cm^{-2} (Fig. 6A); they were found to be equal to 3.26 F cm^{-2} and 407 F g^{-1}, respectively. By comparison of these results to literature data, we have found that the latter value is 2.5 times higher than that reported earlier [37] and over 4 times higher in comparison to the more recent data [38] (Table 3). Moreover, the value obtained is very close to that determined by the present authors for the regular (i.e. not integrated with DSSC) ruthenium oxide/Nafion™ based electrochemical supercapacitor (Fig. 4). In the above considerations, we have

Table 1
Charging/discharging parameters for integrated photocapacitor under different light intensities.[a]

t_{ch} (s)	Q_{ch} (Ccm^{-2})	U (mV)	j_{dch} (mA cm^{-2})	t_{dch} (s)	U_{dch} (mV)	Q_{dch} (C cm^{-2})	C (F cm^{-2})	C (F g^{-1})	η (%)	CE (%)
100% sunlight										
800	1.64	898	0.8	1800	884	1.44	3.26	407	0.80	87.8
50% sunlight										
1860	1.66	829	0.8	1641	803	1.31	3.26	407	0.56	89.0
10% sunlight										
5850	1.22	762	0.8	1329	746	1.06	2.84	356	0.67	86.7

[a] t_{ch} – photocharging time, Q_{ch} – charge collected during photocharging, U – voltage across supercapacitor at the end of charging, j_{dch} – discharging current density, t_{dch} – discharging time, U_{dch} – discharging voltage (after rest time 60 s), Q_{dch} – charge released during discharging, C – specific capacitance in F per geometric area and mass of one electrode respectively, η – energy conversion efficiency, CE – coulombic efficiency.

Table 2
Collection of photocapacitor parameters determined from series of charging (under full sun) and discharging experiments.[a]

t_{ch} (s)	Q_{ch} (Ccm^{-2})	j_{dch} (mA cm^{-2})	t_{dch} (s)	U_{dch} (mV)	C (Fcm^{-2})	C (Fg^{-1})	η (%)	CE (%)	E (mWh cm^{-2})	P (mW cm^{-2})
800	1.64	0.8	1800	884	3.26	407	0.8	87.8	0.17	0.34
800	1.50	1.6	832	860	3.10	388	0.72	88.7	0.16	0.69
800	1.42	3.2	389	840	2.96	370	0.7	87.3	0.15	1.39
700	1.36	6.4	177	800	2.83	352	0.65	83.1	0.12	2.44
700	1.30	9.6	107	770	2.67	333	0.62	79.2	0.11	3.7
700	1.30	12.8	72	730	2.52	315	0.58	71.0	0.09	4.5

[a] E, P – Energy and power density of supercapacitor. The other symbols as for Table 1.

assumed that photocapacitor was fully charged under illumination with light of 100 mW cm^{-2}.

Capacitance values were further processed in order to determine the photocapacitor's energy (E) and power (P) densities. In calculations, the experimentally measured capacitance, rather than the specific one, was considered as described elsewhere [51]. The values of E and P (per unit area of a capacitor electrode) were as follows: 0.17 mWh cm^{-2} and 0.34 mW cm^{-2}, respectively. It is apparent from Table 3 that our E values are larger in comparison to the referenced data [37,38]. This result is not surprising because the energy of the capacitor is directly proportional to capacitance [51]. On the other hand, our P value was lower than that (0.6 mW cm^{-2} in Table 3) reported earlier for a photocapacitor utilizing poly(3,3-diethyl-3,4-dihydro-2*H*-thieno-[3,4-b][1,4]dioxepine) (PProDOT-Et$_2$) films [38]. But it should be remembered that discharging of the PProDOT based photocapacitor was conducted at current densities as high as 2 mA cm^{-2} thus contributing to the overall power density increase. When the current density of 1.6 mA cm^{-2} was applied to the capacitor part of our photocapacitor, the resulting power density reached 0.69 mW cm^{-2} (Table 2).

We also used a discharging profile (Fig. 6) to estimate the amount of charge released during galvanostatic discharging (Q_{dch}). The obtained value, 1.44 C cm^{-2} (Table 1), served for determination of coulombic efficiency of the cell:

$$CE = 100 \cdot \frac{Q_{dch}}{Q_{ch}} \quad (9)$$

where CE is coulombic efficiency (%), Q_{ch} is charge stored during photocharging (C cm^{-2}), and Q_{dch} stands for charge released during galvanostatic discharging (C cm^{-2}).

The fact that coulombic efficiency has been found to be equal to 87.8% supports the view that most of charge generated in photoelectrochemical reaction (and thus accumulated at the capacitor electrodes) could be released with negligible loss thus making the system very effective system generation and simultaneous accumulation of electrical energy. The result is competitive when compared to those reported elsewhere for similar systems (Table 3) [37,38]. Moreover, a slight decrease of coulombic efficiencies (5–10% depending on the sample) was noticed only during the first charging/discharging cycles. This feature reflected most likely changes in the solar cell performance (initial instability) rather than deficiency of the capacitor operation. This explanation is based on our photocurrent observations during photocharging experiments. It slightly decreased during the first few photocharging cycles and, later, the response was stable. The same observation is true for that solar cell working as a single device, i.e. without capacitor.

Another important factor is the energy conversion efficiency (η) defined by the ratio of the useful output of converted energy to the input. In a case of the integrated DSSC-capacitor system, the following equation can be used (upon assumption the potential-independent capacitance):

Table 3
Comparison of photocapacitor parameters to literature data. Charging was carried out under full sun illumination (100% sunlight).[a]

	This paper	Ref. [37]	Ref. [38]
Q_{ch} (C cm^{-2})	1.64	1.12	2.17
t_{ch} (s)	800	1800	310
j_{pc} (mA cm^{-2})	4	14	7
Q_{dch} (C cm^{-2})	1.44	0.47	0.26
j_{dch} (mA cm^{-2})	0.8	0.047	2
U_{dch} (mV)	884	720	650
t_{dch} (s)	1800	10000	130
C (F cm^{-2})	3.26	1.3	0.78
E (mWh cm^{-2})	0.17	0.047	0.022
P (mW cm^{-2})	0.34	0.02	0.6
CE (%)	87.8	42	12
η (%)	0.80	0.09	0.27

[a] j_{pc} – initial photocurrent density, E_{dch} – discharge energy density. The rest of symbols the same as for Table 1.

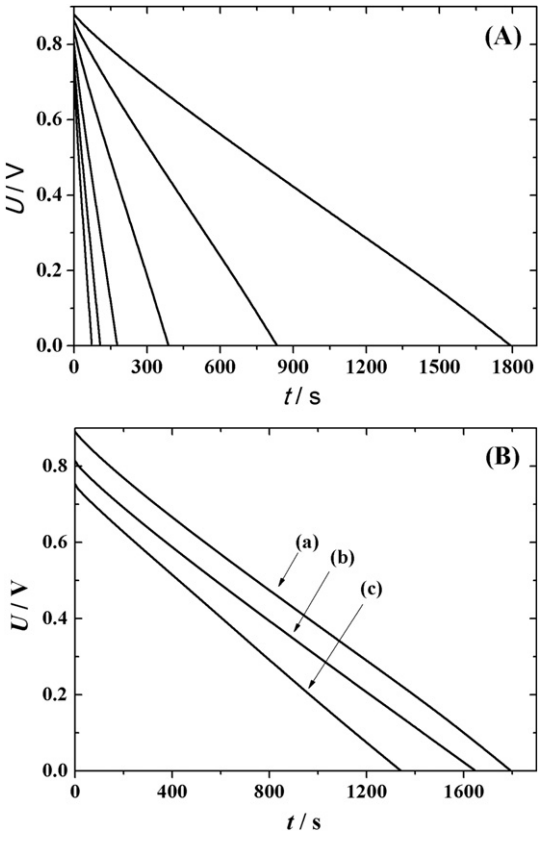

Fig. 6. Discharging of integrated photocapacitor. (A) Monitoring of the capacitor's voltage (U) between the silver electrode and the external counter electrode (Fig. 1) during galvanostatic discharging (in the dark) upon application of increasing (from right to left) current density values: 0.8, 1.6, 3.2, 6.4, 9.6 and 12.8 mA cm^{-2}. Part (B) shows discharging curves at 0.8 mA cm^{-2}. Following photocharging of the capacitor part under different light intensity values: (a) 100, (b) 50, and (c) 10 mW cm^{-2} (equivalent to 100, 50 and 10% of full sun, respectively).

$$\eta = 100 \cdot \frac{E_{out}}{E_{in}} = 100 \cdot \frac{S_{cap}}{S_{DSSC}} \cdot \left(\frac{\frac{1}{2} C_{cap} U_{dch}^2}{P_{in} t_{ch}} \right) \quad (10)$$

where E_{out} and E_{in} stand for the output and input energies (J cm^{-2}); S_{cap} and S_{DSSC} are the areas of electrodes (cm^2) in the capacitor and solar cell parts, C_{cap} is the experimentally measured capacitance (F cm^{-2}) calculated as $i_{dch} \cdot t_{dch}/U_{dch} \cdot m$ at the discharging current density of 0.8 mA cm^{-2}, U_{dch} has been mentioned earlier, P_{in} describes power of the incident light illumination per area of solar cell (W cm^{-2}) and t_{ch} refers to the time of photocharging process (s).

The overall energy conversion efficiency determined using Equation (10) has been equal to 0.8% which is certainly a reasonable result for such an integrated system (Table 3). Our future efforts aim at further improvement of the performance in order to reach the level of at least 3%.

In view of getting a better insight into performance of our integrated photocapacitor, the device was charged again under illumination of 100 mW cm^{-2} and, subsequently, discharged at different current densities ranging from 1.6 to 12.8 mA cm^{-2} (Fig. 6A). The results are summarized in Table 2. Each time photocharging was stopped, the voltage across the capacitor part was ca. 0.9 V. However, when the discharging current density was increased, the discharging voltage decreased due to the appearance of ohmic drops at the beginning of galvanostatic curve. For example, when a very high current density of 12.9 mA was applied, the voltage across the capacitor was equal to 0.73 V after 60 s of rest time, whereas, for lower discharge currents, the discharging process was starting above 0.8 V. Moreover, as was expected, when current density increased, the specific capacitance decreased from 407 at 0.8 mA cm^{-2} to 315 F g^{-1} at 12.8 mA cm^{-2}. Such behavior is characteristic of moderately fast redox systems in which transfers of electrons and protons are not able to follow imposed parameters. Nevertheless, even upon application of the high current load of 12.8 mA cm^{-2}, fairly reasonable values of coulombic and energy conversion efficiencies were maintained, namely 71 and 0.58%, respectively.

Discharging curves recorded for photocapacitor charged under different light intensities are compared in Fig. 6B. The main parameters for those experiments are placed in Table 1. It is important to notice that, even at a low light intensity of 10 mW cm^{-2}, our integrated photocapacitor has been able to reach 0.76 V. After 60 s of rest time, the voltage drops only about 16 mV due to some possible self-discharging and ohmic drops. However, when galvanostatically controlled current density of 0.8 mA cm^{-2} has been applied, the device is still capable of releasing the charge corresponding to a capacitance of 356 F g^{-1} (2.84 F cm^{-2}). Moreover, coulombic efficiency and energy conversion efficiency are still at high level and are equal to 86.7 and 0.67%, respectively. Charging under 50% of sunlight yields results very similar to those obtained for full sunlight (specific capacitance of 407 F g^{-1}, coulombic efficiency of 89%, and energy conversion efficiency of 0.56%). From these data it is possible to state that the proposed design is capable of effective operation under various light conditions.

4. Conclusions

We propose here a novel photoelectrochemical capacitor (photocapacitor) capable of simultaneous energy generation and storage by integrating all solid-state components such as a photorechargeable ruthenium oxide based capacitor and a dye-sensitized solar cell (DSSC). An important issue is to utilize and to couple a photoanode composed of the organic D35 dye-modified titanium oxide together with the polymeric hole conductor, poly-(3-hexylthiophene-2,5-diyl) (P3HT). Separation and interfacing of the charge storage part and the solar cell was achieved with use of an additional bipolar silver electrode (layer).

Attractive capacitive properties of hydrous $RuO_x(OH)_y$ in a symmetric design utilizing a semi-solid type polymer electrolyte (Nafion™ 117) were first verified under voltammetric and galvanostatic conditions. The results are consistent with the system's high specific capacitance of ca. 400 F g^{-1} and fairly fast charging–discharging rates. The material was then successfully coupled with DSSC to yield a well-behaved photoelectrochemical capacitor as an integrated optoelectronic solid-state device. The photocapacitor performance was the best under illumination (photocharging) under full sun (100 mW cm^{-2}) and discharging at 0.8 mA cm^{-2} (0.1 A g^{-1}) to yield coulombic and energy conversion efficiencies equal to 88% and 0.8%, respectively. This result corresponds to specific capacitance of 407 F g^{-1} (3.26 F cm^{-2}) and energy density of 0.17 mWh cm^{-2}. An important issue is that our photocapacitor has not only been able to generate a high photovoltage of 0.88 V but also to convert and store energy even at low incident light intensities such as 10 mW cm^{-2}. The proposed integrated optoelectronics device seems to be suitable to operate under various light conditions including low light intensity.

Acknowledgment

This work was financially supported by the Ministry of Science and Higher Education – National Science Centre, Poland under Project no. N N507 322040, the Foundation for Polish Science (FNP) under Chair (Mistrz) Program and by the Swedish Energy Research Agency Project No.32920-1.

References

[1] B. O'Regan, M. Gratzel, Nature 353 (1991) 737.
[2] F. Gao, Y. Wang, J. Zhang, D. Shi, M. Wang, R. Humphry-Baker, P. Wang, S.M. Zakeeruddin, M. Gratzel, Chem. Commun. 23 (2008) 2635.
[3] A. Yella, H. W Lee, H.N. Tsao, C. Yi, A.K. Chandiran, M.K. Nazeeruddin, E.W.-D. Diau, C.Y. Yeh, S.M. Zakeeruddin, M. Gratzel, Science 334 (2011) 629.
[4] W. Li, J. Kang, X. Li, S. Fang, Y. Lin, G. Wang, X. Xiao, J. Photochem. Photobiol. 170 (2005) 1.
[5] K. Manseki, W. Jarernboon, Y. Youhai, K. J Jiang, K. Suzuki, N. Masaki, Y. Kim, J. Xia, S. Yanagida, Chem. Commun. 47 (2011) 3120.
[6] X. Liu, W. Zhang, S. Uchida, L. Cai, B. Liu, S. Ramakrishna, Adv. Mater. 22 (2010) E150–E155.
[7] Y. Saito, T. Azechi, T. Kitamura, Y. Hasegawa, Y. Wada, S. Yanagida, Coord. Chem. Rev. 248 (2004) 1469.
[8] H.S. Kim, C.C. Wamser, Photochem. Photobiol. Sci. 5 (2006) 955.
[9] Y. Kim, Y.E. Sung, J.B. Xia, M. Lira-Cantu, N. Masaki, S. Yanagida, J. Photochem. Photobiol. A 193 (2008) 77.
[10] A.J. Mozer, Y. Wada, K.J. Jiang, N. Masaki, S. Yanagida, S.N. Mori, Appl. Phys. Lett. 89 (2006) 043509.
[11] Y. Saito, N. Fukuri, R. Senadeera, T. Kitamura, Y. Wada, S. Yanagida, Electrochem. Commun. 6 (2004) 71.
[12] N. Fukuri, N. Masaki, T. Kitamura, Y. Wada, S. Yanagida, J. Phys. Chem. B 110 (2006) 25251.
[13] L. Yang, Z. Zhang, S. Fang, X. Gao, M. Obata, Sol. Energy 81 (2007) 717.
[14] A. Konno, T. Kitagawa, H. Kida, G.R. Asoka Kumara, K. Tennakone, Curr. Appl. Phys. 5 (2005) 149.
[15] V.P.S. Perera, K. Tennakone, Sol. Energy Mater. Sol. Cells 79 (2003) 249.
[16] G.R.R.A. Kumara, A. Konno, G.K.R. Senadeera, P.V.V. Jayaweera, D.B.R.A. De Silva, K. Tennakone, Sol. Energy Mater. Sol. Cells 69 (2001) 195.
[17] B.C. O'Regan, S. Scully, A.C. Mayer, J. Phys. Chem. B 109 (2005) 4616.
[18] U. Bach, D. Lupo, P. Comte, J.E. Moser, F. Weissortel, J. Salbeck, H. Spreitzer, M. Gratzel, Nature 395 (1998) 583.
[19] L. Yang, U.B. Cappel, E.L. Unger, M. Karlsson, K.M. Karlsson, E. Gabrielsson, L. Sun, G. Boschloo, A. Hagfeldt, E.M.J. Johansson, Phys. Chem. Chem. Phys. 14 (2012) 779.
[20] F. Fabregat-Santiago, J. Bisquert, L. Cevey, P. Chen, M. Wang, S.M. Zakeeruddin, M. Gratzel, J. Am. Chem. Soc. 131 (2009) 558.
[21] H.J. Snaith, A.J. Moule, C. Klein, K. Meerholz, R.H. Friend, M. Gratzel, Nano Lett. 7 (2007) 3372.
[22] H.J. Snaith, L. Schmidt-Mende, Adv. Mater. 19 (2007) 3187.
[23] H.J. Snaith, M. Gratzel, Adv. Mater. 19 (2007) 3643.
[24] J.R. Jennings, L.M. Peter, J. Phys. Chem. C 111 (2007) 16100.
[25] I.A. Rutkowska, A. Andrearczyk, S. Zoladek, M. Goral, K. Darowicki, P.J. Kulesza, J. Solid State Electrochem. 15 (2011) 2545.

[26] I.A. Rutkowska, M. Skunik, K. Miecznikowski, P.J. Kulesza, ECS Trans. 13 (2008) 185.
[27] J. Burschka, A. Dualeh, F. Kessler, E. Baranoff, N. Cevey-Ha, C. Yi, M.K. Nazeeruddin, M. Gratzel, J. Am. Chem. Soc. 133 (2011) 18042.
[28] X. Zou, N. Maesako, T. Nomiyama, Y. Horie, T. Miyazaki, Sol. Energy Mater. Sol. Cells 62 (2000) 133.
[29] H. Nagaia, H. Segawa, Chem. Commun. (2004) 974.
[30] A. Hauch, A. Georg, U.O. Krasovec, B. Orel, J. Electrochem. Soc. 149 (2002) A1208.
[31] S. Licht, G. Hodes, R. Tenne, J. Manassen, Nature 326 (1987) 863.
[32] B.E. Conway, J. Electrochem. Soc. 138 (1991) 1539.
[33] M. Jayalakshmi, K. Balasubramanian, Int. J. Electrochem. Sci. 3 (2008) 1196.
[34] G. Wang, L. Zhang, J. Zhang, Chem. Soc. Rev. 41 (2012) 797.
[35] T. Miyasaka, T.N. Murakami, Appl. Phys. Lett. 85 (2004) 3932.
[36] M. Skunik, P.J. Kulesza, N. Vlachopoulos, L. Häggman, A. Hagfeldt, ECS Trans. 35 (2011) 93.
[37] T.N. Murakami, N. Kawashima, T. Miyasaka, Chem. Commun. 26 (2005) 3346.
[38] C.Y. Hsu, H.W. Chen, K.M. Lee, C.W. Hu, K.C. Ho, J. Power Sources 195 (2010) 6232.
[39] H.W. Chen, C.Y. Hsu, J.G. Chen, K. M Lee, C.C. Wang, K.C. Huang, K.C. Ho, J. Power Sources 195 (2010) 6225.
[40] S.M. Feldt, E.A. Gibson, E. Gabrielsson, L. Sun, G. Boschloo, A. Hagfeldt, J. Am. Chem. Soc. 132 (2010) 16714.
[41] J.P. Zheng, P.J. Cygan, T.R. Jow, J. Electrochem. Soc. 142 (1995) 2699.
[42] X. Jiang, M. Quintana, E.M.J. Johansson, M. Karlsson, L. Sun, A. Hagfeldt, G. Boschloo, Adv. Funct. Mater. 21 (2011) 2944.
[43] J.P. Zheng, J. Electrochem. Sol. St. Lett. 2 (1999) 359.
[44] S. Trasatti, G. Lodi, in: S. Trasatti (Ed.), Electrodes of Conductive Metallic Oxides—Part A, Elsevier, New York, 1980, p. 301.
[45] B. Conway, in: The Fourth International Seminar on Double Layer Capacitors and Similar Energy Storage Devices (Dec. 12—14, 1994). Deerfield Beach, FL.
[46] J.P. Zheng, T.R. Jow, J. Electrochem. Soc. 142 (1995) L6.
[47] P.C. Reike, N.E. Vanderborgh, J. Membr. Sci. 32 (1987) 313.
[48] M. Verbrugge, R. Hill, J. Electrochem. Soc. 137 (1990).
[49] M. Verbrugge, E.W. Schneider, R.S. Conell, R. Hill, J. Electrochem. Soc. 139 (1992) 3421.
[50] T.A. Zawodzinski, M. Neeman, L.O. Sillerud, S. Gottesfeld, J. Phys. Chem. 95 (1991) 1040.
[51] M. Skunik, M. Chojak, I.A. Rutkowska, P.J. Kulesza, Electrochim. Acta 53 (2008) 3862.
[52] D.P. Hagberg, X. Jiang, E. Gabrielsson, M. Linder, T. Marinado, T. Brinck, A. Hagfeldt, L. Sun, Mater. Chem. 19 (2009) 7232.